

Galaxy protocluster candidates at $1.6 < z \lesssim 2^*$

Audrey Galametz^{1,2}, Joël Vernet¹, Carlos De Breuck¹, Nina Hatch^{3,4}, George Miley³,
Tadayuki Kodama⁵, Jaron Kurk⁶, Roderik Overzier⁷, Alessandro Rettura⁸,
Huub Röttgering³, Nick Seymour⁹, Bram Venemans¹, and Andrew Zirm¹⁰

¹ European Southern Observatory, Karl-Schwarzschild-Str. 2, D-85748 Garching, Germany [e-mail: agalamet@eso.org]

² Observatoire Astronomique de Strasbourg, 11 rue de l'Université, 67000 Strasbourg, France

³ Leiden Observatory, University of Leiden, P.B. 9513, Leiden 2300 RA, The Netherlands

⁴ University of Nottingham, School of Physics and Astronomy, Nottingham NG7 2RD

⁵ National Astronomical Observatory of Japan, Mitaka, Tokyo 181-8588, Japan

⁶ Max-Planck-Institut für extraterrestrische Physik (MPE), Giessenbachstr.1, D-85748 Garching, Germany

⁷ Max-Planck-Institut für Astrophysik (MPA), D-85748 Garching, Germany

⁸ Department of Physics and Astronomy, University of California, Riverside, CA 92521, USA

⁹ Mullard Space Science Laboratory, UCL, Holmbury St Mary, Dorking, Surrey, RH5 6NT

¹⁰ Dark Cosmology Centre, Niels Bohr Institute, University of Copenhagen, Juliane Mariesvej 30, DK-2100 Copenhagen, Denmark

Preprint online version: August 9, 2010

ABSTRACT

We present a study of protoclusters associated with high redshift radio galaxies. We imaged MRC 1017-220 ($z = 1.77$) and MRC 0156-252 ($z = 2.02$) using the near-infrared wide-field ($7.5' \times 7.5'$) imager VLT/HAWK-I in the Y , H and K_s bands. We present the first deep Y -band galaxy number counts within a large area (~ 200 arcmin²). We then develop a purely near-infrared colour selection technique to isolate galaxies at $1.6 < z < 3$ that may be associated with the two targets, dividing them into (i) red passively evolving or dusty star-forming galaxies or (ii) blue/star-formation dominated galaxies with little or no dust. Both targeted fields show an excess of star-forming galaxies with respect to control fields. No clear overdensity of red galaxies is detected in the surroundings of MRC 1017-220 although the spatial distribution of the red galaxies resembles a filament-like structure within which the radio galaxy is embedded. In contrast, a significant overdensity of red galaxies is detected in the field of MRC 0156-252, ranging from a factor of $\sim 2 - 3$ times the field density at large scales (2.5 Mpc, angular distance) up to a factor of $\sim 3 - 4$ times the field density within a 1 Mpc radius of the radio galaxy. Half of these red galaxies have colours consistent with red sequence models at $z \sim 2$, with a large fraction being bright ($K_s < 21.5$, i.e. massive). In addition, we also find a small group of galaxies within $5''$ of MRC 0156-252 suggesting that the radio galaxy has multiple companions within ~ 50 kpc. We conclude that the field of MRC0156-252 shows many remarkable similarities with the well-studied protocluster surrounding PKS1138-262 ($z=2.16$) suggesting that MRC 0156-252 is associated with a galaxy protocluster at $z \sim 2$.

Key words. large scale structure - galaxies: clusters: general - galaxies: evolution - galaxies: high redshift - galaxies: individuals (MRC 1017-220; MRC 0156-252)

1. Introduction

It is well established that the evolution of galaxies strongly depends on environment. In the nearby Universe, the highest density regions (e.g., the cores of local galaxy clusters) are dominated by red, early-type galaxies with the fraction of blue galaxies with on-going star-formation significantly smaller than lower density regions (Dressler 1980; Tanaka et al. 2005; Postman et al. 2005; Balogh et al. 2007; Poggianti et al. 2009). The spectra of these red passively evolving galaxies show a characteristic break at 4000\AA — i.e., the light from old stellar populations is more prominent than that emitted by younger stars. These galaxies lie on a tight red sequence in colour-magnitude diagrams. Studies have shown that this red sequence is already well populated in clusters of galaxies out to high redshifts ($z \sim 1.5$; Stanford et al. 2005, 2006; Mei et al. 2006, 2009; Lidman et al. 2008; Kurk et al. 2009). To understand when this red sequence appeared, i.e., when the segregation between pas-

sive and star-forming galaxies occurred in clusters, one needs to study overdensities at higher redshifts.

However, the number of known galaxy clusters at high redshifts ($z > 1$) is small. Indeed, searching for higher redshift clusters rapidly becomes challenging using classical detection methods such as using red-sequence algorithms aimed at identifying red galaxy overdensities (Gladders & Yee 2000; Andreon et al. 2008) or detecting the extended X-ray emission from the intra-cluster medium (Stanford et al. 2006; Rosati et al. 2004, 2009). Until recently, the two highest redshift clusters were discovered through X-rays: XMMXCS J2215.9-1738 at $z = 1.457$ (with 17 spectroscopically confirmed members within the cluster virial radius; Stanford et al. 2006; Hilton et al. 2007) and XMMU J2235.3-2557 at $z = 1.39$ (with 34 spectroscopically confirmed members; Rosati et al. 2009). Galaxies in the core of this second cluster already lie on a well defined and tight red sequence (Lidman et al. 2008). These X-ray selected clusters were however recently superseded by the discovery of a galaxy cluster at $z = 1.62$, CIG J0218-0510, using photometric redshifts. It is located in the Subaru/XMM-Newton deep field and has 15

* Based on observations obtained at the European Southern Observatory using the Very Large Telescope on Cerro Paranal through ESO programs 081.A-0673(A) and 083.A-0231(A).

confirmed members to date (Tanaka et al. 2010; Papovich et al. 2010).

One of the most efficient methods to search for galaxy clusters at even higher redshifts ($z > 1.5$) is to look in the vicinity of high-redshift radio galaxies (HzRGs hereafter). These galaxies are among the most massive galaxies in the Universe ($M > 10^{11} M_{\odot}$; Rocca-Volmerange et al. 2004; Seymour et al. 2007) and are good tracers of high density regions in the early universe (see Miley & De Breuck 2008, for a review on HzRGs and their surroundings). Narrow line emitter surveys of HzRGs at $2 < z < 5$ show that they are often located in overdense regions, designated as ‘protoclusters’ that are likely to be the progenitors of the present day massive groups and clusters (Venemans et al. 2002, 2005, 2007; Pentericci et al. 2000; Kurk et al. 2004). The narrow line emitters are, however, only a low-mass subset of the general population of UV-selected, star-forming galaxies (Miley et al. 2004; Overzier et al. 2008) and likely do not represent the majority of the total stellar mass.

Studies have tried to identify more massive cluster galaxies associated with these radio-loud sources by looking for the red passively evolving galaxies that may be populating the cores of high redshift clusters. Best et al. (2003) observed, for example, the environment of powerful radio-loud sources at $z \sim 1.6$ and found overdensities of red galaxies ($R - K > 4$) on two scales around the AGN: a pronounced central peak (within 150 kpc) and weaker excesses between 1 and 1.5 Mpc radius. More recently, Galametz et al. (2009) studied the environment of 7C 1756+6520, a radio galaxy at $z = 1.416$, and found an excess of red sources (passive, early-type galaxy candidates at $z > 1.4$) within 2 Mpc of the HzRG. A galaxy cluster associated with 7C 1756+6520 has since been spectroscopically confirmed (Galametz et al. 2010). At higher redshifts ($z > 2$), studies have searched for red evolved galaxies by bracketing the redshifted 4000Å break with near-infrared filters. Kajisawa et al. (2006) explored the environments of six HzRGs at $z \sim 2.5$ and isolated the evolved galaxy population at $z > 2$ using purely near-infrared (*JHKs*) colour cuts. Kodama et al. (2007) used the same near-infrared criteria to select protocluster member candidates in the field of HzRGs at $2 < z \lesssim 3$ (see also Zirm et al. 2008, for a near-infrared study of a forming red sequence in a protocluster at $z = 2.16$). They both found that some of their targeted fields contained overdensities by a factor of 2 – 3 compared to blank fields. Recent spectroscopic follow-up of these red sources has been conducted in a couple of these protocluster fields by Doherty et al. (2010). They confirm two red galaxies associated with PKS 1138-262 at $z = 2.16$, a dusty star-forming galaxy and an evolved galaxy with little ongoing star formation. These HzRG companions have an estimated mass of $4 - 6 \times 10^{11} M_{\odot}$. Doherty et al. (2010) also confirm that a pure near-infrared criterion is efficient at selecting high redshift galaxies — e.g. 56% of their *JHK*-selected galaxies with spectroscopic redshift fall at $2.3 < z < 3.1$. However, the low success rate of their spectroscopic campaign confirms however the challenge in deriving redshifts for passively evolving galaxies whose spectra do not show prominent and easily identifiable emission lines.

Building on these previous studies of individual HzRG fields, we defined a first uniformly selected sample of the most powerful radio galaxies in the pivotal redshift range $1.7 < z < 2.6$ where we expect the cluster galaxies to start settling on the red sequence. Our method is to select potential cluster members (in particular, evolved passive galaxies) using near-infrared colour cuts. We observed our sample with the High Acuity Wide field K-band Imager (HAWK-I; Pirard et al. 2004; Casali et al. 2006; Kissler-Patig et al. 2008) on the Very Large Telescope

(VLT) in 2008 and 2009 in a set of three filters (*YHKs* or *JHKs* depending on the redshift of the targeted HzRG). This paper reports the results on our two lowest redshift targets. A companion paper presents results on the higher redshift targets (Hatch et al., 2010).

We design a new near-infrared criterion to isolate galaxies at $1.6 < z < 3$. We apply this selection technique to study the galaxy population in the vicinity of the lowest redshift HzRGs of the HAWK-I sample: MRC 1017-220 ($z = 1.77$) and MRC 0156-252 ($z = 2.02$). We first describe in §2 the multi-wavelength data available for the targets and four control fields (including two sub-fields of GOODS South). The extraction of the source catalogues and galaxy number counts are described in §3 and §4. Section 5 presents the colour-colour selection technique we developed to isolate cluster member candidates at $z > 1.6$. The properties of these cluster candidates, such as overdensities and spatial distribution are detailed in §6. Section 7 summarizes our results.

We assume a Λ CDM cosmology with $H_0 = 70 \text{ km s}^{-1} \text{ Mpc}^{-1}$, $\Omega_m = 0.3$ and $\Omega_{\Lambda} = 0.7$. All magnitudes are expressed in the AB photometric system unless stated otherwise.

2. The data

2.1. The targets

We present a study of the two lowest redshifts targets of the HAWK-I sample: MRC 1017-220 and MRC 0156-252, observed with HAWK-I in the *Y*, *H* and *Ks* bands.

MRC 1017-220 ($z = 1.768$; R.A.: 10:19:49.05, Dec.: -22:19:58.03, J2000, $L_{3\text{GHz}} = 10^{28.11} \text{ W Hz}^{-1}$) is our lowest redshift targeted HzRG. We note that this HzRG is a broad line radio galaxy (Kapahi et al. 1998) and is unresolved both in near-infrared and radio (Pentericci et al. 2001). Investigating extremely red objects (EROs; $R - K > 6$) around high- z AGN, Cimatti et al. (2000) found an excess of EROs in the close vicinity of MRC 1017-220 compared to the field.

We also targeted the field around MRC 0156-252 ($z = 2.016$; R.A.: 01:58:33.63, Dec.: -24:59:31.10, $L_{3\text{GHz}} = 10^{27.79} \text{ W Hz}^{-1}$). This HzRG has been reported to be a quasar obscured by dust (Eales & Rawlings 1996; McCarthy et al. 1992).

2.2. Observations and data reduction

2.2.1. New VLT/HAWK-I data

The two HzRG fields were imaged between April 2008 and August 2009 in Service Mode with VLT/HAWK-I. HAWK-I is a wide-field imager on UT4 with a field of view of $7.5' \times 7.5'$ equipped with a mosaic of four Hawaii 2RG 2048 \times 2048 pixel detectors separated by a gap of 15". The pixel scale is 0.1064". The field of MRC 1017-220 was observed in Spring 2008 for 122 min in the *Y* band ($\lambda_C = 10210\text{Å}$), 53 min in the *H* band ($\lambda_C = 16200\text{Å}$) and 33 min in the *Ks* band ($\lambda_C = 21460\text{Å}$). MRC 0156-252 was also observed in the same set of filters: 200 min in the *Y* band (Autumn 2008), 47 min in the *H* band and 33 min in the *Ks* band (August 2009). In order to avoid the gaps between the chips and to have a deeper coverage of the immediate surroundings of the HzRGs, MRC 1017-220 and MRC 0156-252 were placed near the center of one of the chips.

Two control fields (hereafter CF1 and CF2, respectively) centered on R.A.: 11:39:59.66, Dec.: -11:24:29.5 and R.A.: 16:02:06.80, Dec.: -17:25:31.7) were also observed from May to September 2008 in the *Y*, *H* and *Ks* bands.

Table 1. HAWK-I observations

Field	R.A. ^a J2000	Dec. ^a J2000	Band	Exp. Time min	Seeing arcsec	Limit 2σ (3σ)
MRC 1017-220	10:19:54.18	-22:18:27.17	<i>Y</i>	122	0.80	25.91 (25.47)
			<i>H</i>	53	0.63	24.89 (24.45)
			<i>K_s</i>	33	0.55	24.36 (23.92)
MRC 0156-252	01:58:39.16	-25:00:51.01	<i>Y</i>	200	0.54	26.42 (25.98)
			<i>H</i>	47	0.50	24.91 (24.47)
			<i>K_s</i>	33	0.56	24.42 (23.98)
CF1	11:39:59.66	-11:24:29.50	<i>Y</i>	122	0.58	25.80 (25.36)
			<i>H</i>	53	0.52	24.18 (23.74)
CF2	16:02:06.80	-17:25:31.70	<i>Y</i>	122	0.53	25.78 (25.34)
			<i>H</i>	53	0.64	24.90 (24.46)
			<i>K_s</i>	33	0.52	24.35 (23.91)

^a Coordinates are given at the center of the HAWK-I *Y*-band image.

Part of each *Y*-band observation was observed in photometric sky conditions. A standard star, selected from the United Kingdom Infrared Telescope (UKIRT) faint standards list (Hawarden et al. 2001), was observed immediately after the science data to flux calibrate the *Y*-band image.

Between January and March 2008, the entrance window of HAWK-I suffered a degradation and, as a consequence, the shadow of the camera spider became visible on the data. The data thus contain the convolution of the spider shadow with the rotating pupil image, resulting in a cross pattern which repeats the spider symmetry in the background¹. As advised by the HAWK-I User Support Team, we reduced the time for each sub-integration to attenuate the cross pattern. However, some HAWK-I data taken between April and August 2008 show an increase in the sky noise independently of the configuration of the observations and the cross pattern is therefore very hard to subtract (e.g., *H* and *K_s*-bands of CF1). During the data reduction phase, we optimized the subtraction of the cross pattern when removing the background. Unfortunately, the cross pattern in the *K_s*-band of CF1 could not be properly subtracted and the image is unusable.

The data were reduced using the ESO/MVM (or ‘alambic’) reduction pipeline² (Vandame 2004). The image processing followed standard near-infrared reduction steps : dark subtraction, division by normalized sky flats, subtraction of the background, fringing correction and harmonization of the four chip gains. A distortion correction was applied to each chip using stars from the USNO-B1.0 (Monet et al. 2003) catalogue. The images were finally stacked using the same astrometric catalogue (for full details on the pipeline, see Vandame 2004).

2.2.2. Photometric calibration

The *H* and *K_s*-bands were flux calibrated using the 2MASS point source catalogue (Skrutskie et al. 2006) for objects with $11 \leq K \leq 14.5$ (i.e. 22 stars for MRC 1017-220, 13 for MRC 0156-252, 9 for CF1 and 37 for CF2). 2MASS stars total magnitudes were estimated using SExtractor Kron aperture (MAG_AUTO parameter). The derived zeropoints are accurate to 0.06 magnitudes. The 2σ and 3σ detection limits of our im-

¹ See <http://www.eso.org/observing/dfo/quality/HAWKI/Problems/PupilGhosts.html> and <http://www.eso.org/sci/facilities/paranal/instruments/hawki/doc/HAWKI-NEWS-2008-07-11.pdf> for details on the HAWK-I entrance window problem

² <http://archive.eso.org/cms/eso-data/data-packages/eso-mvm-software-package>

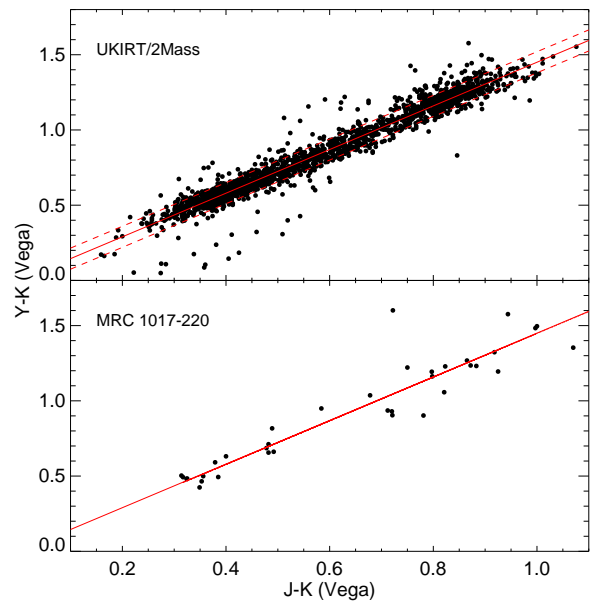


Fig. 1. Colour-colour diagram ($Y - K$ vs $J - K$) for the stars from a combined UKIDSS/2MASS catalogue (top panel) and for the 2MASS stars of the MRC 1017-220 field (bottom panel), shown as an example for the calibration of the *Y*-band HAWK-I data. Stars are well fitted by an empirical colour-colour relation, $(Y - K)_{Vega} = 1.45 \times (J - K)_{Vega}$ (solid line). The standard deviation (0.07) of the distribution is shown by the dotted lines.

ages, determined in randomly distributed $1.5''$ diameter apertures, are reported in Table 1.

We derive the zeropoint of the *Y*-band using the standard stars observations and then refine it using empirically derived near-infrared colour relations for stars. Using the Wide Field Infrared Camera (WFCAM) Science Archive³ which holds images and catalogues of the UKIRT Infrared Deep Sky Surveys (UKIDSS), we retrieve stars from a 1.5×1.5 square degree region (centered around R.A.: 14:00:00, Dec.: 10:00:00) and match the *Y*-photometry of UKIDSS (data release 5) with 2MASS *J* and *K*-photometry. We extract stars with accurate photometry in *Y*, *J* and *K_s* (less than 0.05 magnitude errors; 1707 stars). Fig. 1 (top panel) shows the location of these stars in a $(Y - K)_{Vega}$ vs

³ <http://surveys.roe.ac.uk/wsa/>

$(J - K)_{Vega}$ colour-colour diagram. Both UKIDSS and 2MASS use Vega photometric systems so Vega magnitudes are used in this analysis for consistency. The colour-colour relation for stars is well-fit by a simple linear function $(Y - K)_{Vega} = 1.45 \times (J - K)_{Vega}$ (standard deviation of 0.07). We extract the 2MASS stars from the HzRGs fields and the two control fields and refine the zeropoints previously derived from the standard stars observations using the above colour-colour relation. See the bottom panel of Fig. 1 for an example of the calibration method used for the MRC 1017-220 field. The offsets applied to the initial zeropoint are less than 0.03 mag. We estimate an average 0.06 mag uncertainty in the Y -band photometry of MRC 1017-220, CF1 and CF2 and 0.07 mag for MRC 0156-252. This last field contains fewer stars and thus its photometry is slightly more uncertain. The 2σ and 3σ limiting magnitudes of the Y -band data (determined in random $1.5''$ diameter apertures) are given in Table 1.

2.2.3. Archival GOODS-S data

The Southern field of the Great Observatories Origins Deep Survey (GOODS-S; Dickinson et al. 2003) was observed in J , H and K_s using VLT/ISAAC from October 1999 to January 2007. The data were reduced with the ESO/MVM pipeline by the GOODS team (Retzlaff et al. 2010). The final data release, available since September 2007, includes 24 ISAAC fields in H and 26 ISAAC fields in K_s as well as the final H and K_s combined mosaics⁴ covering respectively 159.6 and 173.1 arcmin².

The GOODS-Multicolor Southern Infrared Catalog⁵ (GOODS-MUSIC; Grazian et al. 2006b; Santini et al. 2009) is a multiwavelength catalogue of GOODS-S, covering 143.2 arcmin² and cross-correlated optical (u , b , v , i , z from Hubble/ACS and VLT/VIMOS), near-infrared (see above), mid-infrared (*Spitzer*/Irac [3.6], [4.5], [5.8], [8.0] and *Spitzer*/MIPS 24 μ m). Spectroscopic redshifts are available for 12% of the sources. GOODS-MUSIC provides photometry for 12 of the 24 fields in H and 22 of the 26 fields in K_s . We make use of the GOODS-MUSIC photometry to calibrate the H and K_s GOODS-S mosaics. The 2σ and 3σ limiting magnitudes in random $1.5''$ diameter aperture are 25.36 (24.92) and 25.20 (24.76) for H and K_s .

As part of the VLT/HAWK-I Science Verification programs, two sub-fields of GOODS-S were observed in Y in December 2007, centered respectively on R.A.: 03:32:40.92, Dec.: -27:51:41.6 (355 min; PI: Fontana, A., GOODS1, hereafter) and R.A.: 03:32:29.71, Dec.: -27:44:38.6 (145 min; PI: Venemans, B., GOODS2, hereafter). See also Castellano et al. (2010) for further details on the data. The seeing of these images is consistent with the one of the ISAAC H and K_s images i.e., $\sim 0.5 - 0.6''$. Fig. 2 shows the K_s -band mosaic of GOODS-S with the H -band (red) and the two Y -band fields, GOODS1 (orange) and GOODS2 (green) overlaid. We reduce the data using ESO/MVM pipeline. The images are astrometrically calibrated using a source catalogue extracted from the GOODS K_s -band mosaic. To flux calibrate the images, we select all objects in the field classified as stellar in the NASA/IPAC Extragalactic Database (NED). Broad band photometry for these stars are taken from the Multiwavelength Survey by Yale-Chile (MUSYC) catalogues (Gawiser et al. 2006). The broad-band SED of the stars are fit using stellar templates from the

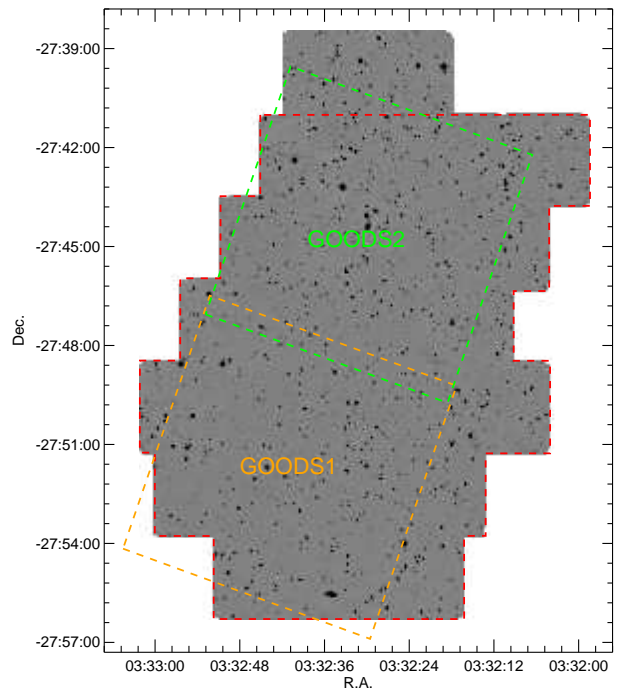


Fig. 2. K_s -band combined mosaic of the 26 tiles observed by VLT/ISAAC in GOODS-S. The 24 fields also observed in H are highlighted by the red dashed line. The two VLT/HAWK-I Y -band observed as part of the science verification of the instrument are overlaid (orange: GOODS1, green: GOODS2).

BPGS spectrophotometric atlas (Hewett et al. 2006). For each star, the best fitting SED provides the Y magnitude of the star and, combined with the flux measured in the image, a zeropoint. The image zeropoint is derived from the average of the individual zeropoints and has an uncertainty of 0.05 magnitudes. We also independently determine the Y -band zeropoint using 2MASS stars in the GOODS-S field (8 stars) and the relation $Y - K = 1.45(J - K)$ used for photometric calibration in §2.2.2 and find results consistent within 0.03 mag. The Y -band 2σ (3σ) limiting magnitudes in random $1.5''$ diameter aperture are 26.94 (26.50) and 26.41 (25.97) for GOODS1 and GOODS2 respectively.

3. Source extraction

HAWK-I data, especially those taken prior to May 2009, contain crosstalk between the amplifiers of the chips i.e., all the sources are repeated on some of the other 32 amplifiers producing a series of crater-like artifacts arrayed horizontally (Finger et al. 2008). Due to its intensity, only crosstalk produced by the brightest objects is observed out of the background, e.g., in the image, all sources with $K_{2MASS,Vega} < 15.5$. Regions affected by crosstalk were masked before extracting the source catalogues. Crosstalk is more prominent in the Y -band since the image is the deepest and stars are brighter in bluer bands. We therefore first identify by eye the crosstalk in the Y -band. A map is created to flag the crosstalk-affected pixels by $4'' \times 4''$ squared masks. The flag area accounts for less than 2% of the final Y images for MRC 1017-220 and CF1 and less than 1% for GOODS-S. The CF2 field contains numerous bright stars and $\sim 4\%$ of the final mosaic is flagged. We also flag regions affected by bright stars

⁴ The reduced single field images and final mosaics are publicly available at http://archive.eso.org/archive/adp/GOODS/ISAAC_imaging_v2.0/goodsreq.html

⁵ Publicly available at <http://lbc.mporzio.astro.it/goods/goods.php>

that dominate their surroundings as well as the noisy edges of the images.

The source detection was performed using SExtractor (Bertin & Arnouts 1996) with a detection threshold of 2σ independently for each filter. We used aperture magnitudes (SExtractor MAG_APER) within a fixed $2.5''$ diameter aperture to measure colours. Based on the profile of stars in the Ks -band data of the HzRGs fields, we estimate that an aperture of $2.5''$ diameter contains about 95% of the source flux. Using such an aperture is therefore a good compromise between including as much flux from the source as possible, but limiting background contamination for faint objects. However, the fraction of a source flux contained in a $2.5''$ aperture strongly depends on the seeing of the image and we smoothed the images of different bands to the same seeing to ensure accurate colour measurements.

The 3-band images of MRC 1017-220 and CF2 have significantly different seeings from filter to filter. We therefore smoothed our images to the worst seeing. The H and Ks -band images of the field of MRC 1017-220 were smoothed to the $0.8''$ seeing of the Y -band. Similarly, the Y and Ks -band images of CF2 were smoothed to the $0.64''$ seeing of the H -band. We detected the sources on the unsmoothed images and determined the aperture photometry on the smoothed images. We explain in §5.3 how we handle upper limits in colours. Total magnitudes are determined using SExtractor parameter MAG_AUTO on the original unsmoothed images.

All magnitudes were corrected for Galactic extinction (calculated for HAWK-I filters) using the dust maps of Schlegel et al. (1998) and assuming $R_V = A_V/E(B - V) = 3.1$ extinction law of Cardelli et al. (1989). All the fields are at high galactic latitude ($b > 20$). Corrections are small for the MRC 1017-220 field (0.054, 0.029, 0.019 mag in Y , H and Ks respectively), the MRC 0156-252 field (0.013, 0.007, 0.004 mag) and CF1 (0.033, 0.018, 0.011 mag). Due to a lot of dust along the line of sight, corrections for CF2 are, on the contrary, rather big (0.344, 0.187, 0.118). We do not apply the negligible (< 0.01 in Y and < 0.005 for H and Ks) extinction corrections for the GOODS-S field.

We evaluated the completeness limits of the images using a IRAF gallist and mkobjects routines (artdata package) to simulate artificial galaxies, both elliptical and spiral galaxies. We chose a uniform distribution of galaxy morphologies with a minimum galaxy axial ratio b/a of 0.8 and a maximum half flux radius of $1''.0$. We adopted a de Vaucouleurs and an exponential disk surface brightness law for ellipticals and spirals respectively. For both types of galaxies, we generated catalogues of 5000 objects and added them to the Y , H and Ks images, including Poisson noise. We determined how many artificial sources were recovered using the same SExtractor configuration files used to detect the real sources. The 90% completeness limits for elliptical (spiral) galaxies are 24.0 (23.3), 22.9 (22.2) and 22.4 (21.7) in Y , H and Ks respectively for MRC 1017-220, 24.4 (23.8), 23.2 (22.5) and 22.4 (21.8) for MRC 0156-252.

4. Galaxy number counts in Y , H and Ks

We derive the differential galaxy number counts in the HzRG fields for each band (see Fig. 3). We only consider the deepest regions of the final images, i.e., we discard the shallowest regions resulting from the gap between chips (central ‘cross’) as well as the edges of the image i.e. 12 – 13% of the images. We also derive the galaxy number counts combining the two control fields: CF1, CF2 and the GOODS-S data for the Y and H bands. For the Ks band, number counts are determined from CF2

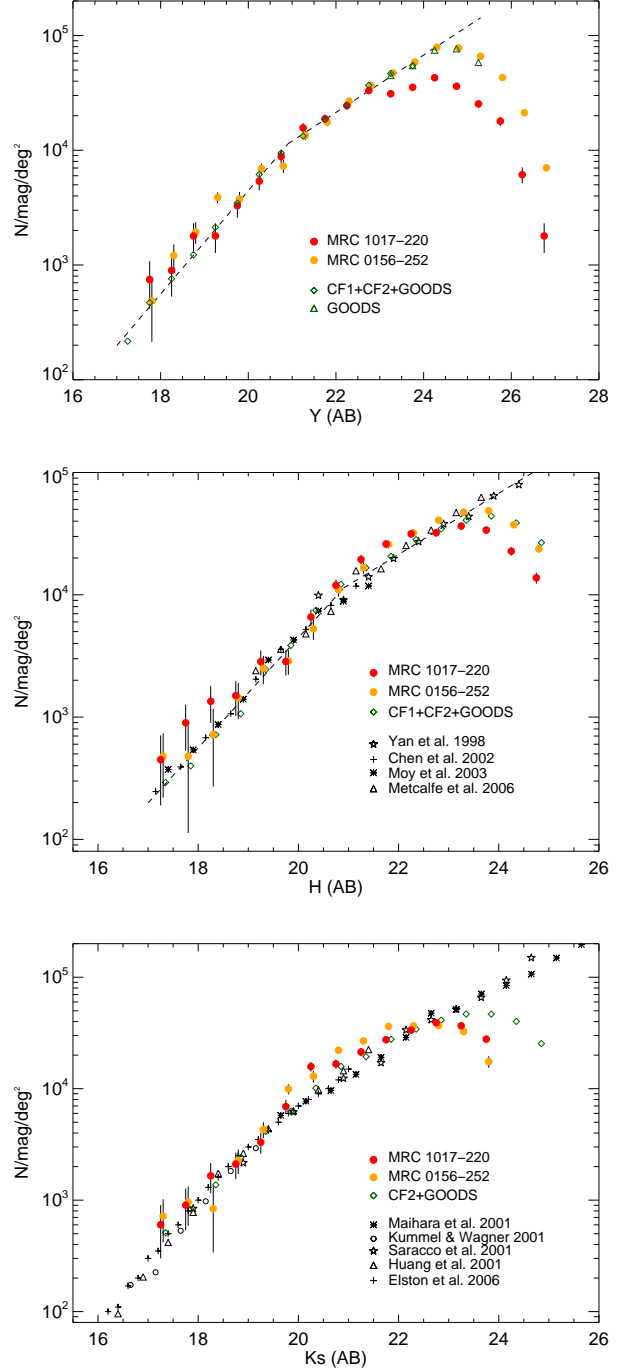


Fig. 3. Galaxy number counts in Y , H and Ks for the field around MRC 1017-220 (red dots), MRC 0156-252 (orange dots) and the combined control fields (green diamonds). We do not apply completeness correction. We isolate galaxies from stars using the stellar index CLASS_STAR in SExtractor. Counts from the literature are overplotted for H and Ks . For the Y -band, we derive counts from the two GOODS-S Y field and the two control fields (CF1 and CF2) until $Y < 24$. Galaxy counts are also derived from GOODS-S only for sources with $23 < Y < 25.5$. The best fit of the Y -band number counts by a two power-law model is shown by the dashed line (see §4, also overplotted on the H -band number counts for comparison).

Table 2. Galaxy number counts in Y -band ($N/(\text{mag.deg}^2)$)

Mag. (1)	1017 (2)	0156 (3)	CFs+GOODS-S (4)	GOODS-S (5)
17.75	747	485	470	-
18.25	896	1213	759	-
18.75	1792	1940	1228	-
19.25	1792	3881	2131	-
19.75	3286	3759	3468	-
20.25	5377	6913	6141	-
20.75	8812	7276	9464	-
21.25	15682	13461	13293	-
21.75	18818	17585	18531	-
22.25	24494	26801	24816	-
22.75	33156	36746	36845	-
23.25	31066	47054	46742	44807
23.75	35397	58817	54652	54695
24.25	-	78948	-	74609
24.75	-	-	-	76683

and GOODS-S, since CF1 was not observed in Ks . We separate galaxies from stars using the SExtractor CLASS_STAR parameter. We test the optimal values for this parameter for each image with stars from 2MASS and USNO in flux bins of 1 mag ($0.6 < \text{CLASS_STAR} < 0.9$).

Table 2 reports (for the first time) the Y -band galaxy number counts. Counts for the two HzRGs fields (columns 2 and 3) are given to the 90% completeness limit. Due to the lower completeness limits of CF1 and CF2, we first derive counts for $Y < 24$ from the four fields (CF1+CF2+GOODS1+GOODS2) i.e., a total area of about 200 arcmin² (see Table 2, column 4). We also derive the counts for $23 < Y < 25.5$ from GOODS-S only (column 5).

For the two other bands, we compare the galaxy counts with results from the literature: Yan et al. (1998); Chen et al. (2002); Moy et al. (2003); Metcalfe et al. (2006) for H and Maihara et al. (2001); Kümmel & Wagner (2001); Saracco et al. (2001); Huang et al. (2001); Elston et al. (2006) for Ks . No attempt is made to correct for the incompleteness, nor correct for differences of filter passbands (e.g., K or Ks).

Number counts have been frequently used to test models of galaxy evolution. Although such an analysis is beyond the scope of this paper, we note however that the slope shown by the Y -band counts is consistent with the H -band. Imai et al. (2007) fitted their J -band counts (derived from the AKARI North Ecliptic Pole survey) by two power-laws of the form $N(\text{mag}) = a \times 10^{b(\text{mag}-15)}$ with a break in the slope at $J_{\text{Vega}} \sim 19.5$. Adopting a similar fitting function, we find that the Y -band counts are well fitted by two power-laws: $a = 25 \pm 5$; $b = 0.45 \pm 0.02$ for $Y < 21$ and $a = 380 \pm 5$; $b = 0.25 \pm 0.02$ for $Y > 21$. These best-fit slopes are plotted in Fig.3 (top panel) and overplotted on the H -band counts (middle panel) for comparison. The Y and H -band counts are found to be consistent. Similarly to Imai et al. (2007), we note that the Ks -band number counts show a less abrupt change of slope at $19 < K < 21$ and cannot easily be modeled by two power-laws.

As shown in Fig. 3 (top panel), the Y number counts of the HzRG fields are in good agreement with counts derived from the control fields. We note that there is a deficit of sources in the MRC 1017-220 field at $Y > 23$, which cannot be explained by a lack of depth of the data since the 90% completeness limit is reached at $Y = 24$ mag. Interestingly, the galaxy counts of the targeted HzRG fields show an excess of galaxies in H for $20.5 < H < 22.5$ where we find $27.1 \pm 0.6\%$ ($22.3 \pm 0.6\%$)

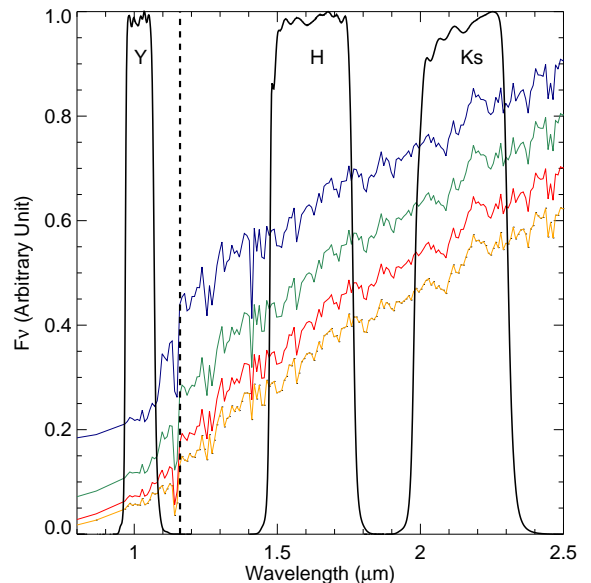


Fig. 4. Redshifted (to $z = 1.9$) spectral energy distribution of models of 2 Gyr-old galaxies assuming an exponential declining star formation history with $\tau = 0.1, 0.3, 0.5$ and 1 (from yellow to blue; see Fig. 5 for colours). The transmission curves of the HAWK-I filters Y , H and Ks and the position of the restframe 4000\AA break (dashed line) are overlaid.

more sources in the field of MRC 1017-220 (MRC 0156-252) than our control fields (CF1+CF2+GOODS). Similar results are found in the Ks -band number counts where an excess of sources with $19.5 < Ks < 22.5$ ($27.4 \pm 0.4\%$) is found in the field of MRC 0156-252 compared to our control fields (CF2+GOODS). An excess of sources with $19.5 < Ks < 21.5$ ($17.8 \pm 0.6\%$) is also seen in the field of MRC 1017-220. We do not observe such excesses in the Y -band (which is below the 4000\AA break at $z \sim 2$). This suggests that both HzRG fields contain an excess of red galaxies.

5. Search for candidate cluster members at $z \sim 2$

5.1. YHK colour selection of galaxies at $z > 1.6$

Colour criteria efficiently select high-redshift galaxies in a relatively narrow redshift range and permit to isolate potential cluster members associated with HzRGs. At high redshifts ($2 \lesssim z \lesssim 3$), the position of the 4000\AA break in galaxies falls between the J and H -band. Pure near-infrared colours have thus been used to isolate candidate protocluster members at this redshift range, e.g. $(J - K)_{\text{Vega}} > 2.3$, designed by the FIRES team (Franx et al. 2003) which allows them to select Distant Red Galaxies (DRGs). However, these single colour cuts mostly pick out red passively evolving or dusty galaxies and miss galaxies with continuous star-formation with little or no dust.

Kajisawa et al. (2006) defined a two-colour selection technique that combined J , H and K colours to select both red, passive and blue, star-forming galaxies at $z > 2$. This criterion $(J - K > 2 \times (H - K) + 0.5 \ \& \ J - K > 1.5; \text{Vega system})$ is almost insensitive to dust extinction since the reddening vector $(E(B - V))$ is parallel to the colour selection.

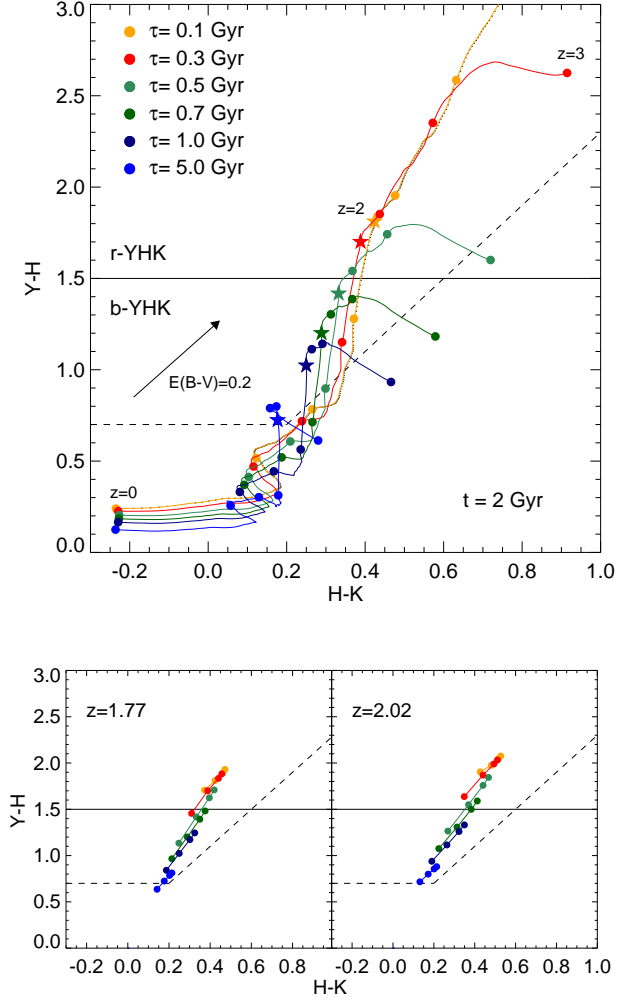


Fig. 5. Bruzual & Charlot (2003) model predictions of different stellar populations in a $Y-H$ vs $H-K$ colour-colour diagram (see text for details on the models). The dashed line accounts for the two-colour selection designed to isolate galaxies at $z > 1.6$. The horizontal line ($Y-H > 1.5$) shows the single-colour selection to separate red passively evolving galaxies (r- YHK galaxies) from star-forming ones (b- YHK galaxies). We assume an exponential declining star formation history with $\tau = 0.1, 0.3, 0.5, 0.7, 1$ and 5 Gyr (see legend). *Top:* for increasing redshifts ($z = 0$ to $z = 3$, each 0.5 bin marked by coloured points) and a constant age of 2 Gyr, the stars corresponding to $z = 1.77$. The black arrow indicates the reddening vector $E(B-V) = 0.2$ as parameterized by Cardelli et al. (1989). *Bottom:* for various population ages ($t = 1.5, 2, 2.5, 2.75$ Gyr, coloured points with $Y-H$ getting redder with ages) at $z = 1.77$ and $z = 2.02$.

At the redshift of the targeted HzRGs, the 4000\AA break is between the Y and the J -band. One can therefore use the Y -band instead of the J -band in a similar method to Kajisawa et al. (2006) to search for cluster members around MRC 1017-220 and MRC 0156-252. We use Bruzual & Charlot (2003) models to determine the colours of different stellar populations at $z = 1.77$ and $z = 2.02$. In the models, we assume a solar metallicity and a Chabrier (2003) initial mass function. Fig. 4 shows dust-free SED predictions for galaxies with an exponentially declining star formation history with $\tau = 0.1$ to $\tau = 1$ Gyr at $z = 1.9$. The HAWK-I transmission filters (black curves) and the position of

the 4000\AA break at $z = 1.9$ (dashed line) are also overlaid. We note that the Y and H filters bracket *restframe* 4000\AA . The Y filter is narrow (width= $0.1\mu\text{m}$, about 3 times narrower than H and K_s). The $Y-H$ colour is therefore very sensitive at selecting galaxies at the targeted redshifts.

Fig. 5 shows the same Bruzual & Charlot (2003) SED models in a $Y-H$ vs $H-K$ colour-colour diagram at various redshifts, with a constant population age of 2 Gyr (top panel), or at various population ages ($t = 1.5$ to 2.75 Gyr) at $z = 1.77$ and $z = 2.02$ (bottom panel). At $z = 0$, galaxies have consistently low $Y-H$ colours ($0 < Y-H < 0.3$). Beyond $z \sim 1.4$, the $Y-H$ colour becomes redder when the 4000\AA break enters the Y -band. The $H-K$ colour stays almost constant until $z \sim 2.5$ when the 4000\AA break enters the H band. By $z > 3$, the $Y-H$ ($H-K$) colour becomes rapidly bluer (redder) than those of galaxies at $1.5 < z < 3$. This general trend is observed for all models. However, the variations on both the $Y-H$ and $H-K$ colours are more pronounced for galaxies with short declining star-formation histories i.e. those with stronger 4000\AA breaks. Galaxies with $\tau < 0.5$ Gyr and $z > 1.6$ have $Y-H > 1.5$. Galaxies with longer star-formation histories never become so red.

We define a new colour criterion, analogous to the Kajisawa et al. (2006) two-colour JHK selection technique, to select galaxies at $1.6 < z < 3$ (Fig. 5, dashed line):

$$Y-H \geq 0.7 \cap Y-H \geq 2 \times (H-K) + 0.3 \quad (1)$$

A single-colour criterion is defined to separate red galaxies with old stellar population from blue star-forming galaxies:

$$Y-H \geq 1.5 \quad (2)$$

similar to the single-colour criterion $(J-K)_{Vega} > 2.3$ that selects DRGs at $z > 2$. This criterion is shown in Fig. 5 as the horizontal solid line. The cut at $Y-H = 1.5$ was optimized to isolate the reddest population of galaxies at $z > 1.6$. By analogy with Kodama et al. (2007) notations (r- JHK and b- JHK) for galaxies selected by the Kajisawa et al. (2006) near-infrared criteria, galaxies selected by equations (1)+(2) are referred to as r- YHK galaxies and galaxies selected by equation (1) with $Y-H < 1.5$ are referred to as b- YHK galaxies.

The YHK criterion is insensitive to dust extinction since it has been defined parallel to the reddening vector $E(B-V)$ (see Fig. 5; black arrow). However, the dusty star-forming galaxies at $z > 1.6$ will have similar colours to non dusty, passively evolving galaxies, and will also be selected by the r- YHK criterion. Our criterion therefore does not enable us to clearly distinguish the red passive galaxies from the dusty star-forming ones.

5.2. Reliability of the YHK colour selection

We examine the YHK colours of galaxies in GOODS-S using the spectroscopic redshifts available in the GOODS-MUSIC catalogue (see §2.2.2) and combining the two archival Y -band (GOODS1 and GOODS2) images with the H and K_s GOODS-S mosaics. We select sources that have a reliable photometry in H and K_s (less than 0.1 magnitude errors), are detected (2σ) in the two Y -band images, and have a reliable spectroscopic redshift (flag 0: very good or 1: good). Fig. 6 (top panel) shows the distribution of these sources in the YHK colour-colour diagram i.e., 72 stars (stars), 316 galaxies at $z < 1.6$ (black dots), 20 galaxies with $1.6 < z < 2.1$ (orange circles) and 10 galaxies with $z > 2.1$ (red circles). AGN (defined as ‘BLAGN’ or ‘NLGN’ in GOODS-MUSIC) are not considered here. We

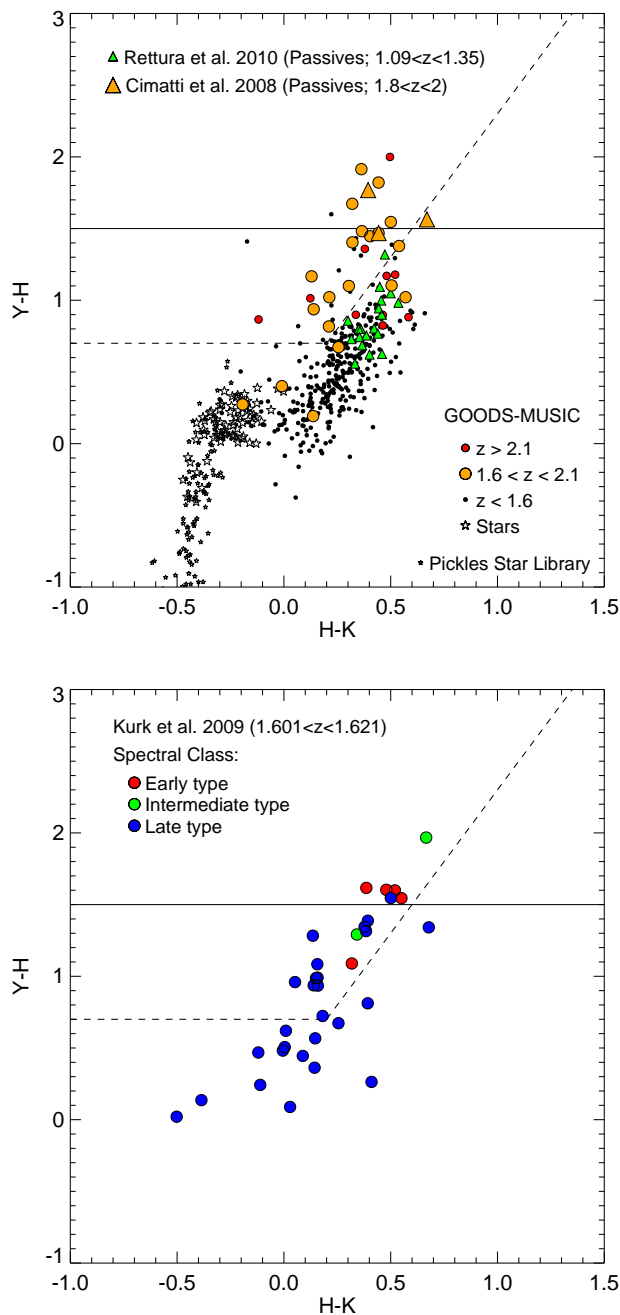


Fig. 6. *YHK* colour-colour diagrams of sources with spectroscopic redshifts from the literature (GOODS-S field). The selection criteria (1) and (2) are shown by the dashed and solid horizontal lines respectively. *Top*: Sources with spectroscopic redshifts from the GOODS-MUSIC catalogue (see legend for symbols) and stars from the Pickles 1998 stellar spectra flux library. We overplot early-type galaxies from Rettura et al. (2010) at $z < 1.5$ as well as the three passive galaxies at $z > 1.8$ from Cimatti et al. (2008) (green and orange triangles respectively). *Bottom*: Members of the overdensity at $z \sim 1.6$ found in GOODS-S (Kurk et al. 2009). Colours of the symbols account for the spectral class of the group members: red, green and blue for early-type, early-type with signs of star formation and late type galaxies respectively.

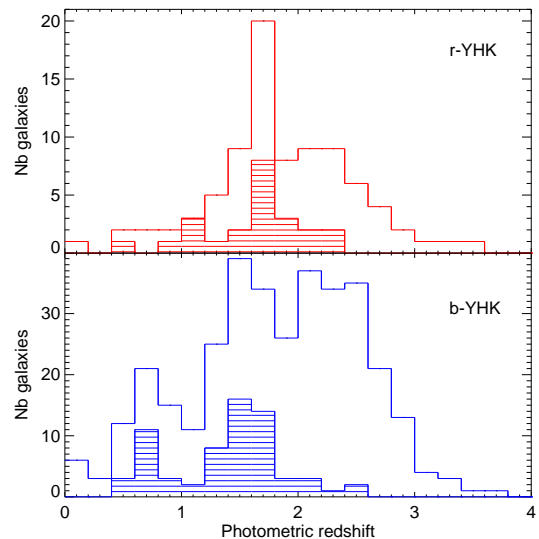


Fig. 7. Photometric redshift distribution of the *YHK*-selected sources for r-*YHK* galaxies (top panel) and b-*YHK* galaxies (bottom panel) in GOODS1+GOODS2 for both the 2σ detection limits (solid histogram) and the limit of completeness of the HAWK-I data (filled histogram). Photometric redshifts are from Santini et al. 2009.

also overplot colours of stars from the digital stellar spectra library from Pickles (1998). We note that 13/20 (65%) galaxies at $1.6 < z < 2.1$ are selected by the *YHK* criteria. The criterion efficiently removes foreground galaxies i.e., only 14/316 ($< 5\%$) galaxies with $z < 1.6$ are found in the *YHK*-selected region. 4/10 (40%) of galaxies with $z > 2.1$ are selected by the *YHK* criterion indicating that the selection will be notably contaminated by background objects.

Rettura et al. (2010) present a sample of 27 early-type galaxies with $1.09 < z < 1.35$ found in the GOODS-S field. 18 of them are imaged and detected ($> 2\sigma$) in the *Y* band (see green triangles in Fig. 6) and have colours consistent with models predictions. Only one of them (the highest redshift source at $z = 1.35$) is selected by the *YHK* criterion showing that contamination by lower redshift passively evolving galaxies is very small.

Cimatti et al. (2008) studied a sample of 13 old, passive galaxies at $z > 1.4$ found in the northern part of GOODS-S covered by the Galaxy Mass Assembly ultra-deep Spectroscopic Survey (GMASS; Kurk et al. 2008). Ten of these objects have $z > 1.6$ including three at $z > 1.8$. The seven others are part of an overdensity at $z \sim 1.6$ presented in Kurk et al. (2009). The three passive galaxies at $z > 1.8$ are well detected in *Y* (in the GOODS2 field), *H* and *K_s* (see orange triangles in Fig. 6, top panel). Two of them have $Y - H > 1.5$. The third one is a b-*YHK* galaxy, but has a red $Y - H$ colour, close to the selection limit.

Kurk et al. (2009) discovered a galaxy overdensity at $z = 1.6$, with 42 spectroscopically confirmed members in the GMASS area. Five galaxies have an early-type spectral class, two galaxies are at an intermediate stage (early-type but with sign of star formation; intermediate type, hereafter) and 35 are late type galaxies. All 42 members are detected in the GOODS2 *Y*-band. Eight late-type galaxies have magnitude errors larger than 0.1 mag in either *Y*, *H* or *K_s* and will not be considered in our analysis. Fig. 6 (bottom panel) shows the colours of the 34 remaining

sources in the *YHK* colour-colour diagram, the colours of the symbols indicating their spectral class.

The five early-type galaxies and the two ‘intermediate type’ galaxies are also reported in Cimatti et al. (2008) as passive galaxies. All seven sources are selected by the *YHK* criterion. Four early-type and one ‘intermediate type’ are r-*YHK* galaxies and the last two sources are b-*YHK* galaxies. 12/27 (44%) of the late type galaxies are selected by the criterion showing its limitation at $z \leq 1.6$. We also note that the [OII] λ 3727Å doublet falls in the *Y*-band at $1.6 < z < 2$. If present, and has a large equivalent width, the emission line could bias the source *Y*-band magnitude and thus its $Y - H$ colour, with the galaxy appearing bluer than expected. Since the majority ($> 80\%$) of the late-type galaxies from Kurk et al. (2009) shows the [OII] line in their spectra, this could explain the blue colours of some of them.

We further test the *YHK* criterion using the photometric redshifts (z_{phot} ; hereafter) available in the GOODS-MUSIC catalogue. Using the multiwavelength photometry of the GOODS-S field, Grazian et al. (2006b) applied a photometric redshift code to their catalogue. They tested their code with the available spectroscopic redshifts and found an accuracy of $\sigma_z = 0.03 \times (1 + z)$ (Grazian et al. 2006a).

We examine the z_{phot} of the *YHK*-selected galaxies within the 2σ detection limits as well as within the 90% completeness limits of the HAWK-I data i.e., the completeness of passive red ellipticals for the r-*YHK* galaxies and the completeness of spiral galaxies for the b-*YHK* galaxies. Fig. 7 shows the photometric redshift distribution of the r-*YHK* galaxies (top panel) and the b-*YHK* galaxies (bottom panel). We find that 77% (2σ ; 71% in the completeness limits) of the r-*YHK* galaxies and 68% (47%) of the b-*YHK* have $z_{phot} > 1.6$ which confirms the efficiency of the selection criteria.

The r-*YHK* criterion is efficient at selecting galaxies at the targeted redshifts with 42% (50%) of the sources with $1.6 < z_{phot} < 2.1$. Within the limits of completeness, the b-*YHK* criterion is also efficient with 38% of galaxies having $1.6 < z_{phot} < 2.1$. The photometric redshift distribution becomes much broader when considering fainter sources and extends towards higher redshift sources. At the 2σ limits, 27% of b-*YHK* sources have $1.6 < z < 2.1$. We note that if indeed an overdensity of red or blue galaxies is present in the surroundings of the HzRGs, the sample of *YHK*-selected galaxies in these fields would contain a higher fraction of sources at the targeted redshifts. The percentages given earlier are therefore expected to be lower limits.

5.3. The *YHK*-selected galaxies

We apply the *YHK* criteria to the five fields with *YHK* coverage i.e., MRC 1017-220, MRC 0156-252, CF2, GOODS1 and GOODS2. We consider sources with a 2σ detection in all three bands. The $Y - H$ vs $H - K$ colour-colour diagrams for the five fields are shown in Fig. 8. Red and blue circles indicate r-*YHK* and b-*YHK* galaxies respectively.

We overplot sources detected (within 2σ limits) in *H* and *Ks* but not in our *Y*-band catalogue. In order to place these sources in the colour-colour diagram, we assume a lower limit on the *Y*-band magnitude (see arrows, Fig. 8). We use SExtractor in dual mode using the source positions in the *Ks*-band and deriving aperture photometry for these sources on the *Y*-band. For sources brighter than our 2σ detection limits but that were not part of our *Y*-band catalogue (i.e. beyond our completeness limits), we assign the *Y*-band photometry derived from the aperture placed at the *Ks*-band source position. For fainter sources, we assign

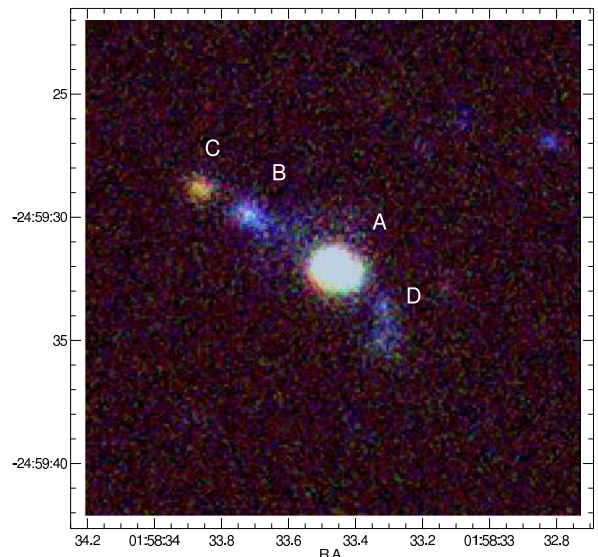


Fig. 9. 3-colour image (R, G, B for *Ks*, *H*, *Y*) of the $20'' \times 20''$ field of view around MRC 0156-252 (North is Up, East Left). A is the radio galaxy. B and C, previously reported in Pentericci et al. 2001, are respectively selected by the r-*YHK* and b-*YHK* criterion. An additional component, D, is also found aligned with MRC 0156-252, B and C but too faint in *Ks* to be classified by our near-infrared criterion.

them the 2σ limits of our *Y*-band images. Sources with lower limits falling in the r-*YHK* selection area of the colour-colour diagram are overplotted in red. These objects are particularly interesting since they have very red $Y - H$ colours which suggests they have strong 4000Å breaks.

Within our 2σ limits in *Y*, *H* and *Ks*, we find 38 r-*YHK* galaxies (151 b-*YHK* galaxies) in MRC 1017-220, 105 (191) in MRC 0156-252, 47 (196) in GOODS1, 48 (176) in GOODS2 and 38 (81) in CF2. We note that since the 2σ magnitude limits and area slightly vary from field to field, these numbers are not directly comparable to one another.

Cimatti et al. (2000) looked at the populations of EROs ($(R - K)_{Vega} > 6$) in 14 fields around radio-loud AGN at $z > 1.5$, including MRC 1017-220. An excess of EROs was found in the field of MRC 1017-220, with three EROs located within $2.5'$ of the HzRG. Two of the three were observed in spectroscopy in the *H*-band with VLT/ISAAC (Cimatti et al. 1999) and a ‘spectrophotometric’ redshift (z_{spect}) was derived for both sources combining the ISAAC spectrum continuum and broad-band photometry. The two sources, J101948-2219.8 (R.A.: 10:19:47.79, Dec.: -22:19:46.6, $K_{Vega} = 18.7$, $z_{spect} = 1.52 \pm 0.12$) and J101950-2220.9 (R.A.: 10:19:49.76, Dec.: -22:20:53.9, $K_{Vega} = 18.6$, $z_{spect} = 1.50 \pm 0.25$), were both classified as early-type galaxies due to their SEDs consistent with no dust extinction. We look at the colours of these two objects (see black squares, Fig. 8, bottom left panel) and both are selected by the b-*YHK* criterion. However, only deeper spectroscopy over a wider wavelength range will confirm whether those two targets have redshifts consistent with MRC 1017-220.

Pentericci et al. (2001) presented near-infrared NICMOS imaging of MRC 0156-252. They found two objects within $5''$ of the radio galaxy, the three sources being aligned in the direction of the radio axis (i.e. NE/SW). Fig. 9 is a three-colour image of the close vicinity of MRC 0156-252. Three objects are observed near MRC 0156-252. We label the components using the

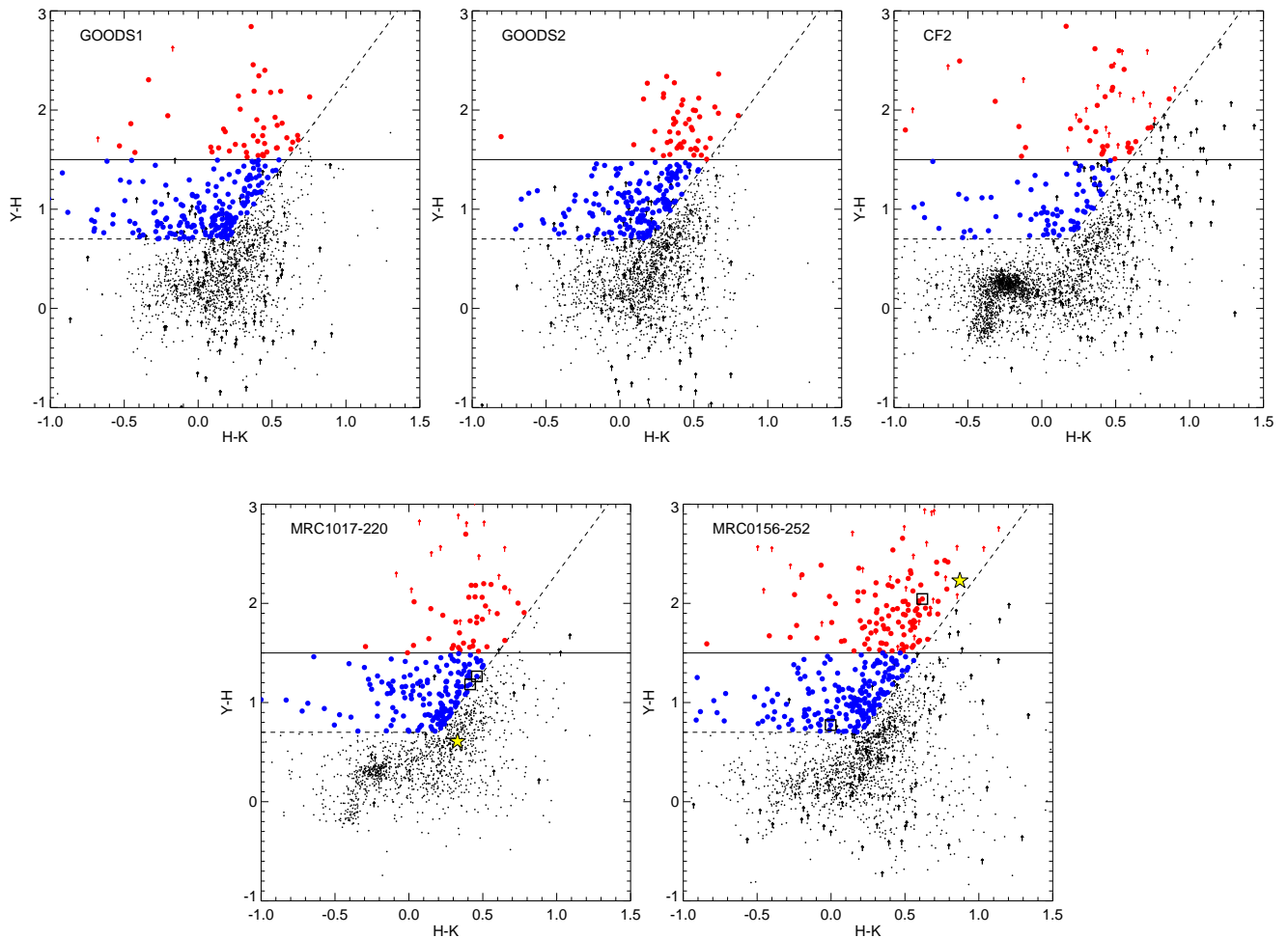


Fig. 8. Colour-colour diagrams $Y-H$ vs $H-K$ for all the fields : *Top panels*: Control fields: GOODS1 (left), GOODS2 (middle) and CF2 (right). *Bottom panels*: HzRG fields: MRC 1017-220 (left) and MRC 0156-252 (right). We plot galaxies detected down to the 2σ detection limits in Y , H and K_s (black dots). r - YHK and b - YHK galaxies are designed by red and blue circles. Arrows indicate lower limits for sources detected in H and K_s but not in Y . The radio galaxies are marked by the yellow stars in the bottom panels. We also indicate with black open squares the two EROs found in the field of MRC 1017-220 (bottom left panel, Cimatti et al. 1999) and the two sources found within $5''$ of MRC 0156-252 (bottom right panel) corresponding to objects B (the b - YHK galaxy) and C (the r - YHK galaxy) in Fig. 9.

same notation as Pentericci et al. (2001) (A for MRC 0156-252, B and C for the two eastern components), adding ‘D’ for the third faint source to the west of the HzRG. As previously noticed in Pentericci et al. (2001), component C is much redder than component B. C is a r - YHK galaxy and B is a b - YHK galaxy. B and C are indicated by black squares in Fig. 8, bottom right panel. D is detected but is very faint in K_s ($< 2\sigma$ level) and was therefore not considered in the candidate selection process. Spectroscopy is required to prove the association of these objects with the radio galaxy but their physical closeness and colours strongly suggest that they are associated with MRC 0156-252. The scale of this system is similar to the structure associated with PKS 1138-262 i.e., about $15''$ (see Miley et al. 2006, Fig. 2).

6. Candidates properties

6.1. Surface densities of YHK -selected galaxies

We compare the surface densities of the YHK -selected galaxies in the five fields to determine whether there is an overdensity of sources around the targeted HzRGs. For a direct field to field comparison, we cut the catalogues at the completeness limits of the shallowest HAWK-I images (see §3; $Y < 24$, $H < 22.9$ and $K_s < 22.4$). Table 3 summarizes the densities for both the r - YHK and b - YHK galaxies in the five fields assuming Poisson errors for the source densities.

As far as the r - YHK galaxies are concerned, the fields around MRC 1017-220, CF2 and GOODS1 have similar densities. As expected, GOODS2 which contains the overdensity at $z = 1.6$ described in Kurk et al. (2009) is slightly denser than average, e.g. by a factor of 1.7 ± 0.7 compared to GOODS1. The field around MRC 0156-252 is significantly overdense compared to all the other fields: by a factor of 3.1 ± 1.1 compared to

Table 3. Number densities of *YHK*-selected galaxies

Field	Area (arcmin ²)	r- <i>YHK</i> ^a (deg ²)	b- <i>YHK</i> ^a (deg ²)
MRC1017-220	54.9	720 ± 220	2530 ± 410
MRC1017-220 (< 1Mpc)	11.0	1800 ± 770	3240 ± 1030
MRC0156-252	59.0	2220 ± 370	2010 ± 350
MRC0156-252 (< 1Mpc)	11.0	2520 ± 910	1800 ± 770
CF2	54.3	930 ± 250	1460 ± 310
GOODS1	50.3	640 ± 210	1570 ± 340
GOODS2	50.3	1070 ± 280	1790 ± 360

^a Within 90% completeness limits; densities were rounded for clarity.

MRC 1017-220, 3.5 ± 1.3 compared to GOODS1 and 2.1 ± 0.6 compared to GOODS2⁶.

We also derive densities within 1 Mpc ($\sim 2'$, angular separation) for both HzRGs corresponding to the classical estimates of virial radius in the highest redshift clusters known to date (e.g. Hilton et al. 2007). In the close vicinity of MRC 0156-252, the r-*YHK* density is even higher: 3.9 ± 1.9 times denser than GOODS1 and 2.4 ± 1.1 times denser than the (overdense) GOODS2 field.

As far as the b-*YHK* galaxies are concerned, densities are more similar from field to field. However, we find that GOODS2 and the HzRGs fields are slightly denser than average. MRC 1017-220 is the densest field. The region within 1 Mpc of the radio galaxy is 2.2 ± 0.8 times denser than CF2. The field of MRC 0156-252 is also denser, by a factor of 1.4 ± 0.4 compared to CF2.

We also derive the number counts of the *YHK*-selected galaxies in all the targeted fields. Reference number counts are derived for both r-*YHK* and b-*YHK* selected galaxies combining CF2, GOODS1, GOODS2 and subtracted from the number counts of the targeted HzRGs fields. Fig. 10 illustrates the number counts of this ‘excess’ of *YHK* galaxies per 0.5 K_s mag bin suspected to be associated with the HzRGs. Errors on both the radio galaxies fields and reference fields number counts are added in quadrature. We assume the Gehrels (1986) small numbers approximation for Poisson distributions.

As for Table.3, this analysis is made in the limits of completeness of the (shallowest) data for a direct field to field comparison. However, due to the selection technique combined with our completeness limits, we do not select all *YHK* galaxies in the fields with the selection getting rapidly incomplete at fainter magnitudes. To illustrate this, we look at the colours of r-*YHK* galaxies in the field of MRC 0156-252. On average, they have $\langle H - K_s \rangle \sim 0.4$ and $\langle Y - H \rangle \sim 1.7$. The completeness limit in *Y* (our limiting band) is $Y = 24$ corresponding to $H = 22.3$ and therefore $K_s = 21.9$, despite the data being complete up to half a magnitude deeper in K_s . We therefore limit the analysis to $K_s < 22$.

No significant excess is seen in the r-*YHK* number counts of the MRC 1017-220 field compared to the control fields. The excess of b-*YHK*, already mentioned earlier in this section is also observed in Fig. 10 with an excess of $K_s > 20.5$ sources. The field of MRC 0156-252 also shows an excess of blue $K_s > 20$ sources. We do not observe an excess of bright red sources

⁶ The *YHK* colour selection is very sensitive to the photometric calibration of the images and the *Y*-band zeropoint has relatively large error bars (0.07). We note however that even if the zeropoint was offset by -0.07, the field would still be overdense in red galaxies by a factor of 2.4 compared to MRC 1017-220 and 1.6 compared to GOODS2.

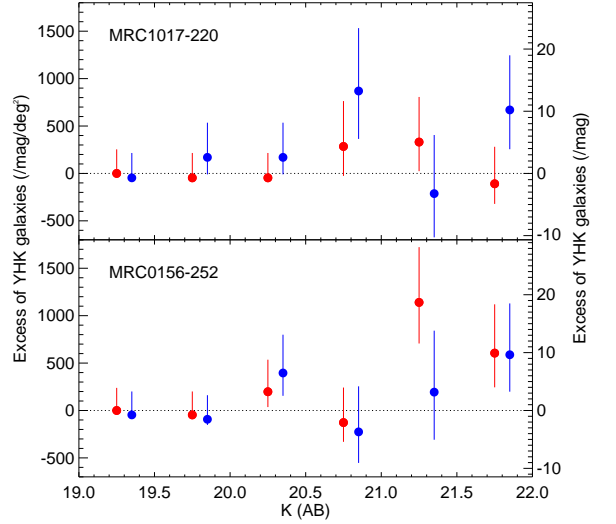


Fig. 10. Number counts of the excess of *YHK*-selected galaxies (per 0.5 K_s mag bin) found in the surroundings of MRC 1017-220 (top panel) and MRC 0156-252 (bottom panel). We first derive reference number counts for the r-*YHK* (red) and b-*YHK* (blue) galaxies from the control fields: CF2+GOODS1+GOODS2 and then subtract them from the number counts of the *YHK* galaxies found in the field of the HzRGs. We assume poissonian errors. Densities are given in sq. deg. (left axis). Excess number of galaxies for each HzRG field (~ 60 sq. arcmin) is shown on the right axis.

($K_s < 20$) in the field of MRC 0156-252 as compared to the control fields. The overdensity of red sources in the field of MRC 0156-252 becomes prominent at $K_s > 21$ with an excess of 10 to 20 galaxies in the field (by bin of 0.5mag) compared to average. At $z \sim 2$, such magnitudes in K_s for elliptical galaxies correspond to masses of several $10^{11} M_\odot$ (Kodama et al. 2007; Rocca-Volmerange et al. 2004) suggesting that if the overdensity detected is indeed associated with MRC 0156-252, the HzRG would lie in a structure that already contains very massive, passively evolving galaxies.

6.2. Spatial distribution of the candidates

The spatial distribution of the *YHK*-selected galaxies (detected within our 2σ magnitude limits) in the two GOODS fields is shown in Fig. 11 for r-*YHK* and b-*YHK* galaxies in red and blue large circles. Sources detected in *Y*, *H* and K_s (2σ) are marked with black dots. Sources detected in *H* and K_s but not in *Y*, though falling in the r-*YHK* selection area (i.e. red arrows in Fig. 8), are overplotted in small red dots. Due to the deep GOODS *Y*-band, there are only two such sources. We observe a clear inhomogeneity in the distributions of r-*YHK* and b-*YHK* galaxies in the northern part of the field (GOODS2). A concentration of both red and blue galaxies is found at the location of the $z = 1.6$ galaxy overdensity presented in Kurk et al. (2009), confirming again the efficiency of the *YHK* criterion at detecting $z \geq 1.6$ galaxy structures.

We note that the northern part of GOODS1 (the southern part of the GOODS field) is more populated with r-*YHK* galaxies than the rest of GOODS1. The spatial distribution of b-*YHK* galaxies is more homogenous, but we also observe a clear concentration of b-*YHK* galaxies at the same position as

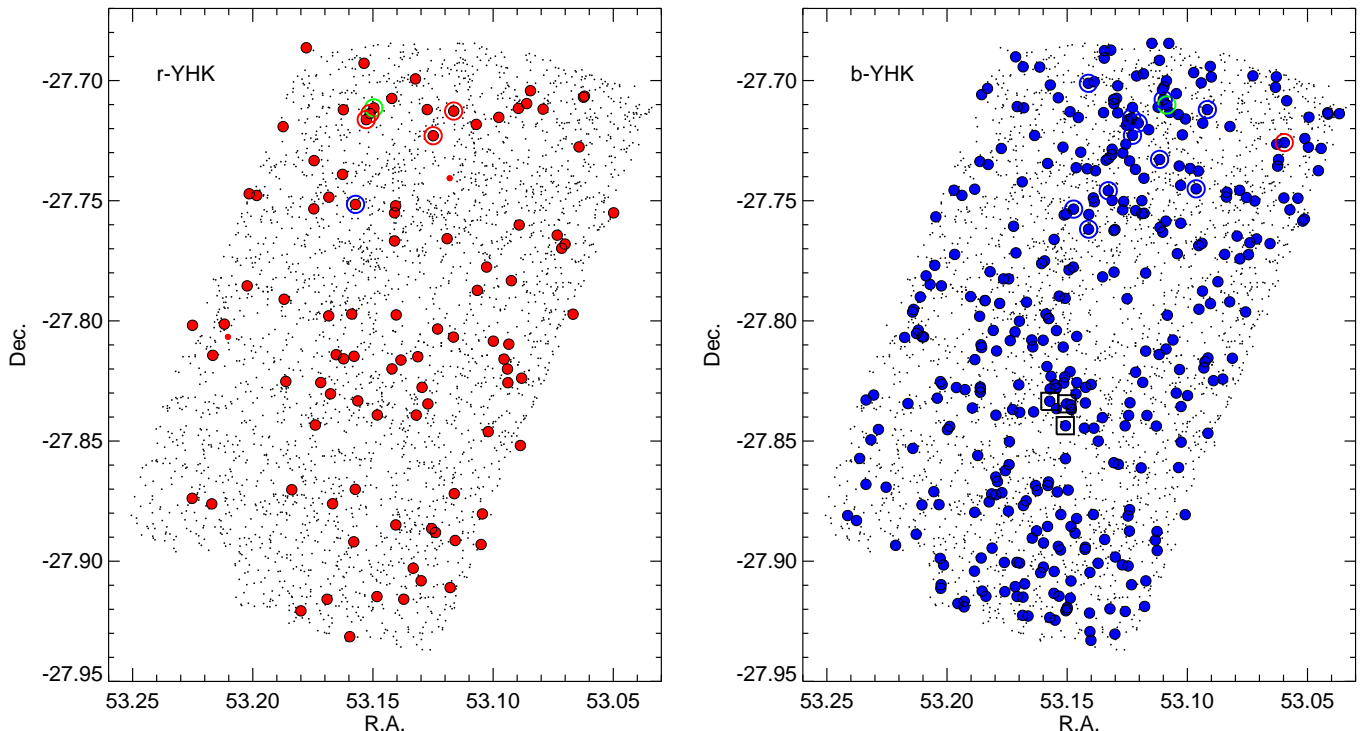


Fig. 11. Spatial distribution of the *YHK*-selected galaxies in the GOODS fields (GOODS1+GOODS2). We also indicate with open circles the 6 *r-YHK* and 12 *b-YHK* galaxies, spectroscopically confirmed members of the overdensity at $z \sim 1.6$ reported by Kurk et al. (2009), symbols colours accounting for the object spectral class (see Fig. 6, lower panel). Three *b-YHK* galaxies confirmed at $z \sim 1.6$ from the ESO GOODS spectroscopy are also indicated by black squares.

the excess of *r-YHK* galaxies (i.e. at R.A. ~ 53.15 and Dec. ~ -27.83). We therefore confirm the results of Kurk et al. (2009) and Castellano et al. (2007) that the overdensity spreads southward. Three of the *b-YHK* galaxies have a spectroscopically confirmed redshift of ~ 1.6 from the ESO GOODS spectroscopy (reported in the GOODS-MUSIC catalogue; see the three black squares in Fig. 11, right panel).

The spatial distribution of the *YHK* galaxies around MRC 1017-220, MRC 0156-252 and in CF2 is shown in Fig. 12. *r-YHK* and *b-YHK* galaxies are shown as red and blue large circles (first and second column) respectively. Sources detected in *H* and *Ks* with lower limits in *Y* and selected by our *r-YHK* criteria are shown by small red dots. Distances from both HzRGs (yellow star) are indicated on the top and right axis of the four first panels. We do not see any specific distribution of *YHK*-selected galaxies in CF2 (Fig. 12, bottom row).

For MRC 1017-220, we indicate the two EROs with spectro-photometric redshift from Cimatti et al. (1999) by black squares. The *r-YHK*-selected galaxies have a non uniform spatial distribution over the field, with a hint of a filamentary distribution in the NW-SE direction in which lies the radio galaxy. No clear spatial inhomogeneity is observed for the *b-YHK* galaxies except a slight excess in the southern part of the field. We note that this result is in agreement with previous studies which show that red galaxies are more strongly clustered than blue ones (Daddi et al. 2000; Brown et al. 2003; Kong et al. 2006).

A visual inspection of the field around MRC 0156-252 confirms the overdensity of red objects around the HzRG, with the *r-YHK* being more concentrated around the HzRG. A concentration of *b-YHK* galaxies is seen in the immediate ($r < 2'$) North-West of the HzRG. A second concentration of blue galaxies is

also observed in the South-East part of the field (at R.A. ~ 29.66 - 29.70 , Dec ~ -25.05). However, no counterpart of this blue galaxy excess is seen in the *r-YHK* galaxy distribution.

6.3. The colour-magnitude diagram

The distribution of the candidates in the $Y - H$ vs Ks colour-magnitude diagram is shown in Fig. 13. Red and blue filled circles indicate *r-YHK* and *b-YHK* galaxies respectively. Candidates in the close vicinity of the HzRGs ($r < 2'$ corresponding to 1 Mpc at the HzRG redshifts) are shown by larger circles in the bottom panels. Both HzRGs are marked by yellow stars⁷. We overplot the expected location of a sequence of passively evolving galaxies (taken from the Coma cluster at $z = 0$) at $z = 1.77$ and $z = 2.02$ for three different formation redshifts ($z_f = 3, 4$ and 5). Models at $z = 1.6$ are also overplotted as the GOODS colour-magnitude diagrams (top panels) since a galaxy structure at $z = 1.6$ is known to lie in these fields (see §5.1).

The right insets of each panel give the histogram of the $Y - H$ colours of the candidates galaxies at $z > 1.6$. It is now well known that galaxies in clusters show a strong bimodality in their colour distribution, with star-forming non-dusty galaxies being on the bluer side, and passively evolving galaxies on the redder side (corresponding to the location of the red sequence) separated by a ‘green valley’ of intermediate type objects. A bimodal repartition is suggested in the histograms of the two HzRGs (lower panels) with two peaks on both sides of $Y - H \sim 1.5$

⁷ We note that at the redshift of MRC 1017-220 ($z = 1.77$), the [OII] $\lambda 3727\text{\AA}$ line is falling in the *Y* band which can explain the very blue $Y - H$ colour of the HzRG.

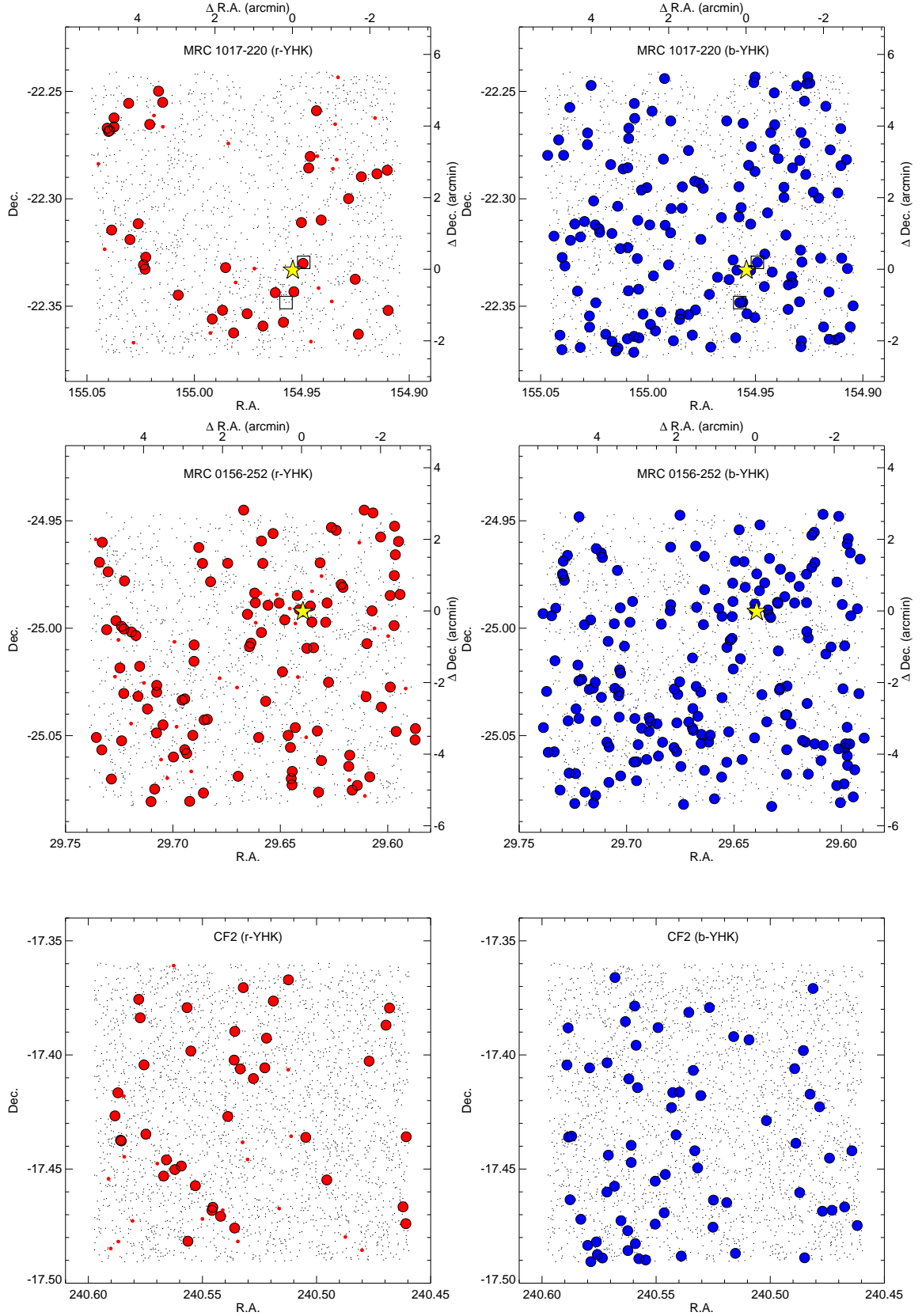


Fig. 12. Spatial distribution of the *YHK*-selected galaxies in the fields around MRC 1017-220 and MRC 0156-252 and the control field CF2: b-*YHK* galaxies in blue and r-*YHK* galaxies in red (arrows of Fig. 8 in small red dots).

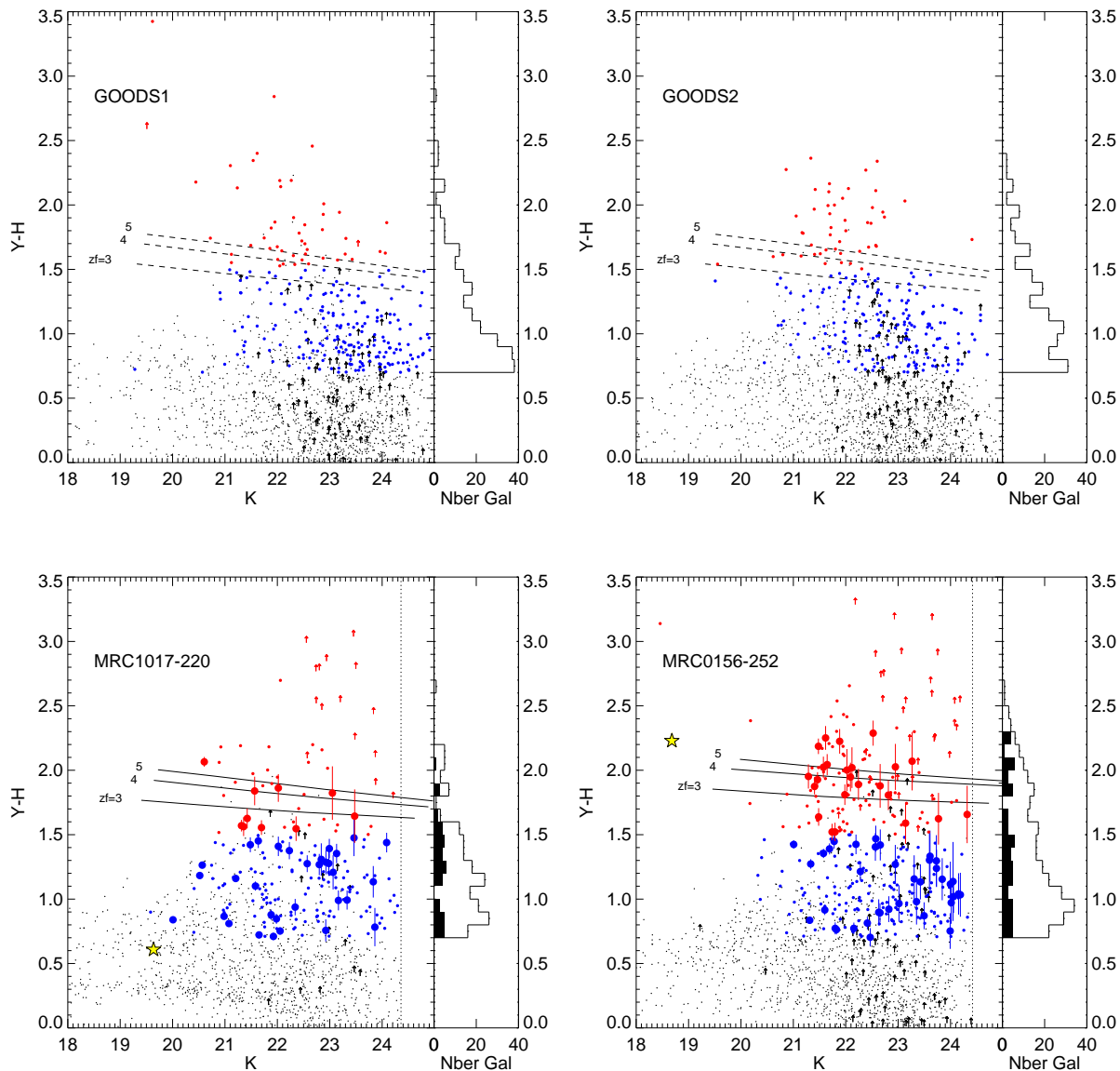


Fig. 13. Colour-magnitude diagrams ($Y - H$ vs K) of the two GOODS fields and the environments of the HzRGs. The r - YHK and b - YHK galaxies are marked by red and blue dots. YHK galaxies within 1 Mpc of the HzRGs are highlighted by bigger symbols and error bars in the two lower panels. The yellow stars indicate the radio galaxies. The 2σ detection limit of the K_s bands are shown by the dotted lines. Models of a red sequence at $z = 1.77$ and $z = 2.02$ are overplotted in the bottom left and right panels respectively (solid lines). For information, models of red sequence at $z = 1.6$ are also overplotted in the GOODS panels — corresponding to the redshift of the galaxy structure confirmed by Kurk et al. (2009) in the GOODS field (dashed lines). Models indicate the predicted colours of a passively evolving stellar population ($z_f = 3, 4$ and 5 from bottom to top). We also show on the right side of each plot, the histogram of the $Y - H$ colours of all the candidate cluster members (both red and blue galaxies; open histograms). The filled histograms (two lower panels) correspond to YHK -selected galaxies within 1 Mpc of the HzRGs.

corresponding to the separation criteria that was designed to isolate passively evolving galaxies from star-forming blue ones.

Half of the red sources within 1 Mpc of MRC 0156-252 have colours consistent with red sequence-like galaxies at $z = 2.02$. The scatter of these sources is quite large (over 0.4mag), the intrinsic scatter being enlarged by errors on the Y -band photometry, and contamination from background/foreground galaxies. If some of the red galaxies are indeed passively evolving galaxies at $z \sim 2$, they would have been formed at very high redshift with a formation redshift $z_f > 3$.

We also note similarities between the colour-magnitude diagram of MRC 0156-252 and that of PKS 1138-262 presented in Kodama et al. (2007). The r - YHK galaxies that lie on the red sequence models in the field of MRC 0156-252 have $21 < K < 23$ with a high fraction of them ($\sim 40\%$) lying on the brighter end ($21 < K < 21.5$). This is consistent with the field around PKS 1138-262, where the majority of the red near-infrared selected sources ($(J - K)_{Vega} > 2.3$) which lay on the red sequence had $20.5 < K < 23$ and half of them had $K < 21.5$. This suggests that both fields contain massive red galaxies.

At $z \sim 2$, the 4000Å break enters the J -band. J -band spectroscopy is thus necessary to prove that the red galaxies are indeed associated with MRC 0156-252. Kriek et al. (2008) present a near-infrared spectroscopic survey of 36 K -bright galaxies ($K_{Vega} < 19.7$) at $z_{phot} > 2$ selected from the Multi-wavelength Survey by Yale-Chile (MUSYC; Gawiser et al. 2006; Quadri et al. 2007) and derive spectroscopic redshifts for their full sample ($1.6 < z_{spec} < 2.73$). Such a spectroscopic campaign could be conducted similarly in the field of MRC 0156-252 since it contains 23 r- YHK (22% of the r- YHK sample) and 18 b- YHK galaxies (13% of the b- YHK sample) which have $K < 21.5$.

Doherty et al. (2010) describe a spectroscopic campaign in the PKS 1138-262 field. Two DRGs were confirmed to lie at the redshift of the radio galaxy (due to the presence of the $H\alpha$ emission line in their spectra). One is a dust-obscured star-forming, red, galaxy. The other is an evolved galaxy with little on-going star formation. These are the first spectroscopically confirmed red galaxies associated with a protocluster at $z > 2$. These results are encouraging for a future near-IR spectroscopic campaign in the field of MRC 0156-252.

7. Summary

We develop a new purely near-infrared YHK 2-colour selection technique to isolate galaxies at $z > 1.6$ and classify them as (i) passively evolving, or dusty star-forming galaxies and (ii) star-forming dominated galaxies with little or no dust. We test the method using the GOODS-South field, which has been observed in Y , H and K_s , and for which a large amount of spectroscopic data is available. GOODS-S contains a structure of galaxies at $z \sim 1.6$ (42 spectroscopically confirmed members so far). Applying the near-infrared criteria to the GOODS-S field, we recover this structure confirming the efficiency of our new selection technique.

We target the surroundings of two high redshift radio galaxies, MRC 1017-220 ($z = 1.77$) and MRC 0156-252 ($z = 2.02$) and a control field using VLT/HAWK-I. The field of MRC 1017-220 shows a non-homogeneous filamentary-like spatial arrangement of red galaxies, and a slight overdensity of blue galaxies. MRC 0156-252 lies in an overdense region of both blue and red galaxies. This field is 2 – 4 times denser than the other targeted fields.

The red galaxies are clustered around MRC 0156-252 (< 1 Mpc). The blue galaxies seem to be preferentially distributed in two regions; a concentration of b- YHK galaxies is found immediately at the NW of MRC 0156-252 and another concentration is found in the SE part of the field, $4'$ (~ 2 Mpc at $z = 2$) away from the HzRG. Our study of the close vicinity of MRC 0156-252 suggests that the radio galaxy has close-by companions with three galaxies found aligned with the HzRG (and the radio axis) and within $5''$. This structure is similar to the system found in the vicinity of PKS 1138-262.

The distribution of the selected red galaxies in a colour-magnitude diagram shows that a large fraction of them have colours consistent with red sequence-like objects (with $z_f > 3$, assuming they contain no dust). The magnitude range of these candidates is also similar to the red protocluster members selected in the vicinity of PKS 1138-262, with red galaxies preferentially lying on the bright end ($K < 21.5$). This suggests that the systems associated with the HzRGs have already formed their more massive members. All these results strongly suggest that MRC 0156-252 is associated with a galaxy structure at $z = 2$

similar to the galaxy system associated with PKS1138-262 at $z = 2.16$.

References

- Andreone, S., Maughan, B., Trinchieri, G., & Kurk, J. 2008, arXiv:0812.1699
- Balogh, M. L. et al. 2007, MNRAS, 374, 1169
- Bertin, E. & Arnouts, S. 1996, A&AS, 117, 393
- Best, P. N. et al. 2003, MNRAS, 343, 1
- Brown, M. J. I. et al. 2003, ApJ, 597, 225
- Bruzual, G. & Charlot, S. 2003, MNRAS, 344, 1000
- Cardelli, J. A., Clayton, G. C., & Mathis, J. S. 1989, ApJ, 345, 245
- Casali, M. et al. 2006, in SPIE, Vol. 6269, Society of Photo-Optical Instrumentation Engineers (SPIE) Conference Series
- Castellano, M. et al. 2007, ApJ, 671, 1497
- , 2010, A&A, 511, A260000+
- Chabrier, G. 2003, PASP, 115, 763
- Chen, H.-W. et al. 2002, ApJ, 570, 54
- Cimatti, A. et al. 1999, A&A, 352, L45
- , 2000, MNRAS, 318, 453
- , 2008, A&A, 482, 21
- Daddi, E. et al. 2000, A&A, 361, 535
- Dickinson, M., Giavalisco, M., & GOODS Team. 2003, in The Mass of Galaxies at Low and High Redshift, ed. R. Bender & A. Renzini, 324–+
- Doherty, M. et al. 2010, A&A, 509, 83
- Dressler, A. 1980, ApJ, 236, 351
- Eales, S. A. & Rawlings, S. 1996, ApJ, 460, 68
- Elston, R. J. et al. 2006, ApJ, 639, 816
- Finger, G. et al. 2008, in SPIE, Vol. 7021, Society of Photo-Optical Instrumentation Engineers Conference Series
- Franx, M. et al. 2003, ApJ, 587, L79
- Galametz, A. et al. 2009, A&A, 507, 131
- , 2010, arXiv:1004.3021
- Gawiser, E. et al. 2006, ApJS, 162, 1
- Gehrels, N. 1986, ApJ, 303, 336
- Gladders, M. D. & Yee, H. K. C. 2000, AJ, 120, 2148
- Grazian, A. et al. 2006a, A&A, 453, 507
- , 2006b, A&A, 449, 951
- Hawarden, T. G. et al. 2001, MNRAS, 325, 563
- Hewett, P. C. et al. 2006, MNRAS, 367, 454
- Hilton, M. et al. 2007, ApJ, 670, 1000
- Huang, J.-S. et al. 2001, A&A, 368, 787
- Imai, K. et al. 2007, AJ, 133, 2418
- Kajisawa, M. et al. 2006, MNRAS, 371, 577
- Kapahi, V. K. et al. 1998, ApJS, 118, 275
- Kissler-Patig, M. et al. 2008, A&A, 491, 941
- Kodama, T. et al. 2007, MNRAS, 377, 1717
- Kong, X. et al. 2006, ApJ, 638, 72
- Kriek, M. et al. 2008, ApJ, 677, 219
- Kümmel, M. W. & Wagner, S. J. 2001, A&A, 370, 384
- Kurk, J. et al. 2009, arXiv:0906.4489
- Kurk, J. D. et al. 2004, A&A, 428, 817
- Kurk, J. D. et al. 2008, in Astronomical Society of the Pacific Conference Series, Vol. 381, Infrared Diagnostics of Galaxy Evolution, 303
- Lidman, C. et al. 2008, A&A, 489, 981
- Maihara, T. et al. 2001, PASJ, 53, 25
- McCarthy, P. J., Persson, S. E., & West, S. C. 1992, ApJ, 386, 52
- Mei, S. et al. 2006, ApJ, 644, 759
- , 2009, ApJ, 690, 42
- Metcalfe, N. et al. 2006, MNRAS, 370, 1257
- Miley, G. & De Breuck, C. 2008, A&A Rev., 15, 67
- Miley, G. K. et al. 2004, Nature, 427, 47
- , 2006, ApJ, 650, L29
- Monet, D. G. et al. 2003, AJ, 125, 984
- Moy, E. et al. 2003, A&A, 403, 493
- Overzier, R. A. et al. 2008, ApJ, 673, 143
- Papovich, C. et al. 2010, ApJ, 716, 1503
- Pentericci, L. et al. 2000, A&A, 361, L25
- , 2001, ApJS, 135, 63
- Pickles, A. J. 1998, PASP, 110, 863
- Pirard, J. et al. 2004, in The Society of Photo-Optical Instrumentation Engineers (SPIE) Conference Series, Vol. 5492, Society of Photo-Optical Instrumentation Engineers (SPIE) Conference Series, ed. A. F. M. Moorwood & M. Iye, 1763–1772
- Poggianti, B. M. et al. 2009, ApJ, 697, L137
- Postman, M. et al. 2005, ApJ, 623, 721
- Quadri, R. et al. 2007, AJ, 134, 1103

- Rettura, A. et al. 2010, *ApJ*, 709, 512
Retzlaff, J. et al. 2010, *A&A*, 511, A50+
Rocca-Volmerange, B., Le Borgne, D., De Breuck, C., Fioc, M., & Moy, E. 2004, *A&A*, 415, 931
Rosati, P. et al. 2004, *AJ*, 127, 230
—, 2009, arXiv:0910.1716
Santini, P. et al. 2009, arXiv:0905.0683
Saracco, P. et al. 2001, *A&A*, 375, 1
Schlegel, D. J., Finkbeiner, D. P., & Davis, M. 1998, *ApJ*, 500, 525
Seymour, N. et al. 2007, *ApJS*, 171, 353
Skrutskie, M. F. et al. 2006, *AJ*, 131, 1163
Stanford, S. A. et al. 2005, *ApJ*, 634, L129
—, 2006, *ApJ*, 646, L13
Tanaka, M., Finoguenov, A., & Ueda, Y. 2010, arXiv:1004.3606
Tanaka, M. et al. 2005, *MNRAS*, 362, 268
Vandame, B. 2004, PhD Thesis, Nice University, France
Venemans, B. P. et al. 2002, *ApJ*, 569, L11
—, 2005, *A&A*, 431, 793
—, 2007, *A&A*, 461, 823
Yan, L. et al. 1998, *ApJ*, 503, L19+
Zirm, A. W. et al. 2008, *ApJ*, 680, 224